Generalized Gradient: Basic Principles and Example Application

Vassili Kovalev[1)], Eduard Snezhko [1)] Siarhei Kharuzhyk [2)] and Vitali Liauchuk [1)]
1) Biomedical Image Analysis and Mathematical Cybernetics Depts.
United Institute of Informatics Problems,
Surganova St., 6, 220012 Minsk, Belarus
vassili.kovalev@gmail.com, http://uiip.bas-net.by
2) N.N. Alexandrov National Cancer Center of Belarus,
223043 Minsk, Lesnoy district, Belarus
skharuzhyk@nld.by, http://omr.by

Abstract: *This paper presents a generalized approach for computing image gradient. It is predominantly aimed at detecting unclear and in certain circumstances even completely invisible borders in large 2D and 3D texture images. The method exploits the conventional approach of sliding window. Once two pixel/voxel sets are sub-sampled from orthogonal window halves, they are compared by a suitable technique (e.g., statistical t-test, SVM classifier, comparison of parameters of two distributions) and the resultant measure of difference (e.g., t-value, the classification accuracy, skewness difference of two distributions etc.) is treated as the gradient magnitude. The bootstrap procedure is employed for increasing the accuracy of difference assessment of two pixel/voxel sets.*

Keywords**:** Computed Tomography, Weak Edges, Generalized Gradient

1. INTRUDUCTION

In many occasions, there is a strong need for detection of borders of objects, which look like patterns of random textures. Such borders could be hardly detected by human visual system when textures differ by their high-order statistics only [1], [2]. Recently, some advanced methods of detecting hardly visible borders between the random image textures have been suggested [1], [3]. Moreover, it was experimentally proven that these methods capitalizing on so-called “generalized gradient” are able to highlight the border which is completely invisible for human eye. For example, the problem of weak birders detection may occur while differentiation of malignant tumors and atelectasis (partial collapse of the lungs) on native CT images of thorax [4], [5].

The purpose of this particular paper is to present results of an experimental study of the ability of the generalized gradient method to highlight hardly visible borders of objects. The study was conducted using three different groups of images. They were comprised by 3D synthetic images and specially-designed physical gelatin phantom made by authors and scanned using Siemens Somatom Definition AS tomograph. Finally, the utility of the method was examined on the problem of borders detection between malignant lung tumors and the atelectasis regions based on 3D CT images of 40 lung cancer patients.

The first version of the generalized gradient method was introduced in [2] as so-called classification gradient and slightly improved afterwards. The classification gradient method makes use conventional technique of calculating image gradient at each pixel position by means of comparing pixel/voxel values taken from orthogonal halves of appropriately sized sliding window. However, apart from the traditional approaches where the gradient magnitude is computed simply as the intensity difference (estimated by convolution with one or other matrix of weights), the generalized gradient method treats the voxel values taken from window halves as two samples which need to be compared in a suitable way. Once it is done, the value of the corresponding dissimilarity measure is treated as a “gradient” value at the current sliding window position for a given orientation X, Y or Z. One may prefer to employ a sophisticated technique of comparing two samples of voxels such as the voxel classification procedure performed with the help of an appropriate classifier [3]. In these circumstances, the resultant classification accuracy is treated as the local image gradient magnitude, which is varied in the range of 0-100%. Along with recent classifiers, the sets of voxels may, for example, be compared in a statistical manner using conventional *t*-test. In this case, the resultant *t*-value is treated as a measure of dissimilarity that is as the signed local “gradient” value. It should be noted that despite the fact that *t*-test is also compares mean values of two voxel samples, it is much more sensitive to their differences because it takes into account the variances of two distributions.

2. METHOD

The above informal definition of the generalized gradient presents the essence of the method used in present study. The exact computational procedure is a bit more complicated. A list of key details which needs to be considered for better understanding and correct implementation of the method is given below.

Despite the method may be used for computing generalized gradient maps of 2D images, it is better suited for 3D because it is supposed to deal with relatively larger samples of voxels taken from sliding window halves.

It is clear that with no respect to the nature and underlying mechanism of the procedure used for comparing two voxel sets taken from adjacent window halves, it is highly desirable to have the resultant dissimilarity estimate as precise as possible. In order to achieve this, a bootstrap multi-step meta-procedure can be employed (see, for example, a good tutorial [6] written for non-statisticians). In practice, it particularly means that at each computational step not the whole amount but a fraction of voxels should be sub-sampled in a random manner from window halves for executing chosen comparison procedure such as *t*-test. This step should be repeated about 100 times. Then the final dissimilarity measure is computed as a mean value of corresponding particular dissimilarity values that is as the mean *t*-value computed over the all 100 particular trials in case the *t*-test procedure is employed. The same holds true in case the final clustering accuracy value is calculated based on particular classification steps, *etc*. The natural payment for the increased accuracy of assessing the difference by means of bootstrap is the growth of computational expenses for about two orders. For instance, in case of 3D images the total number of elementary *t*-tests which need to be performed resides around 300 with about 100 tests accomplished for computing gradient components G_x, G_y and G_z along each of three orthogonal image axes X, Y and Z.

Once the generalized gradient components G_x, G_y and G_z are computed using the procedure of voxel set comparison, the gradient magnitude $G^{x,y,z}$ at a particular 3D voxel position (x,y,z) is calculated as the Euclidean norm of the vector. In general, the sliding window may have not three orthogonal orientations of voxel sampling like traditional axes X, Y and Z but some alternative configurations too. In this study, we also utilized a bit more sophisticated configuration of sliding window depicted in Fig.1. It supposes to use six directions equally-spaced in 3D. Sampling in each direction is performed using corresponding spherical sub-windows with radius R. Moreover, the sub-windows are moved apart from the central voxel at the distance d. This was done to address the problem of smooth and wide object borders. The resulting generalized gradient value at a particular 3D voxel position (x,y,z) is calculated from the particular values in each direction G_i, $i \in \{1,...,6\}$ as $G^{x,y,z} = \left(\sum_{i=1}^{6} G_i^2\right)^{1/2}$.

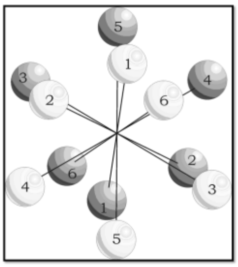

Fig. 1. Configuration of the gap sliding window

3. MATERIALS

In this study we used three kinds of images containing regions with weak borders which are difficult to detect by human visual system: synthetic 3D images, CT image of the physical gelatin phantom and CT images of chest of 40 patients. Image regions did not form coherent spatial pattern, but rather looked like random textures with difference being the probability density functions of values inside them.

3.1 SYNTHETIC IMAGES

For this experiment, we created a synthetic 3D image with size (512 × 512 × 50) voxels. Inside this volume a parallelepiped was placed with distances along the corresponding volume margins equal to 128, 128 and 12 voxels. The grey values of the voxels of the inner and outer regions were drawn from two Pearson distributions with different parameters, having the same mean value of $\mu = 200$ and standard deviation $\sigma = 20$, but different skewness values. The inner part was filled with values to have the skewness ω_{in} to be as close as possible to 1 taken throughout all the image slices, and voxels from the outer part were filled with values to have the global skewness $\omega_{out} = 2$. It should be noted that due to the probabilistic technique of values generation the exact equality of their mean, standard deviation and skewness to the expected ones is hardly possible.

The results are depicted on Fig.2. This experiment shows the capability of the generalized gradient (GG) maps calculated with different presets to detect weak borders, and the results are as they were expected. Fig.2(c) and Fig.2(d) show the clear border between inner and outer regions. We used the SVM classification accuracy as the difference measure improved by the bootstrap procedure and the gap sliding window. No a priory information about border orientation, width, smoothness or values distribution was used.

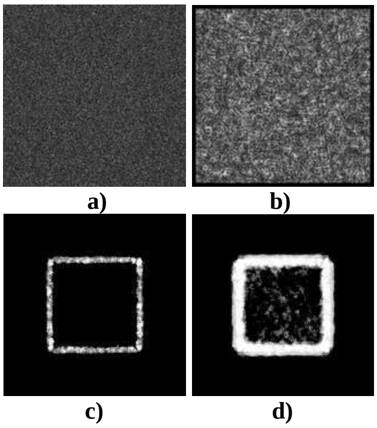

Fig. 2. a) Original synthetic image; b) GG map using *t*-test, R = 4, d = 2; c) GG map using SVM, gap window's R = 3, d = 1; d) GG map using SVM, R = 4, d = 2

Fig.2(b) depicts the GG map calculated using conventional *t*-test to estimate the dissimilarity measure between values sampled from the gap window halves.

Though this map calculation is much faster than of the previous ones, in this particular case it gives no positive outcome, because *t*-test does not react on the difference of skewness and higher orders moments. However, further we will show that it also provides useful results retaining the same relative advance in speed when used for processing of real images.

3.2 PHYSICAL GELATIN PHANTOM

The purpose of creating physical phantom was to obtain CT image of some real object, consisting of several adjacent parts with low relative contrast (layers). The phantom was supposed to simulate the commonly encountered problem when objects present on radiological images have barely visible boundaries.

To create such a phantom, we used a cylindrical container filled with several horizontal layers of gelatin. Different levels of CT brightness of each layer were obtained by means of dissolving certain precalculated amount of radiocontrast agent Omnipaque in liquid gelatin before its solidification. To control the amounts of radiocontrast agent some provisional measurements of Omnipaque solutions' CT-brightness have been made (see Fig.3(a) and Fig.3(b)).

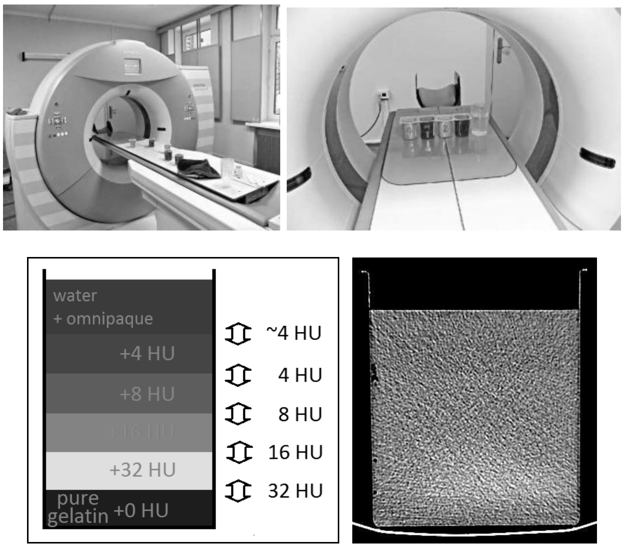

Fig. 3. a) General view of the installation; b) cups with different amounts of dissolved Omnipaque solution at the calibration stage; c) phantom scheme; d) one slice of the phantom CT image.

To the amounts of dissolved Omnipaque solution were chosen to increase pure gelatin (reference) CT-brightness by 4, 8, 16 and 32 Hounsfield unit (HU) for different layers relative to the brightness of the reference layer. The reference layer was located at the most bottom of the container. The brightest layer was placed next, then the others (see Fig.3(c)). Besides, an additional layer of water with Omnipaque solution introduced was poured to the most top. Thus, one more low-contrast border was made between the upper gelatin layer and the liquid layer.

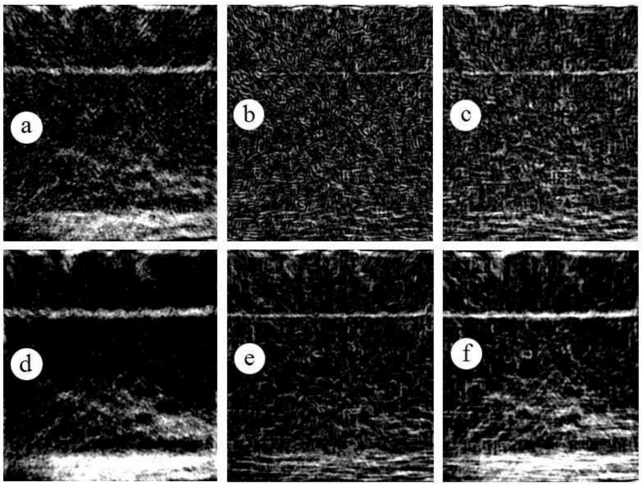

Fig. 4. a), d) – GG maps calculated using gap window with R = 4, d = 2 and R = 5, d = 3 respectively, *t*-test of voxel samples used for dissimilarity measure estimation; b), e) – GG maps calculated using spherical window with r = 5 and r = 8 respectively, *t*-test of voxel samples used for dissimilarity measure estimation; c), f) – GG maps calculated using spherical window, dissimilarity measure is the difference of mean values sampled from window halves.

The resultant GG maps of the image in Fig. 3(d) are depicted in Fig.4. Left column contains maps calculated using *t*-test to estimate dissimilarity measure and gap sliding window, middle column – also *t*-test and spherical sliding window, right column – spherical sliding window and dissimilarity measure is the difference of mean values sampled from window halves. Sizes of all sliding windows along first and second rows were chosen to have almost the same number of voxels. Unlike the previous synthetic images, the gelatin phantom layers have definite differences of mean HU values, that's why it is fairly easy problem to detect weak borders using different presets of the method. Nevertheless, this figure may help to choose the preferable method's parameters depending on the desired result. The middle layers of gelatin seem to be interdiffused and there were no detectable borders.

3.3 MALIGNANT LUNG TUMORS

In this study, we used 40 CT images of thorax of patients with lung cancer and the atelectasis of a portion of the lung as diagnosed by a qualified radiologist and confirmed histologically. Thirty-three of them were males and remaining seven were females. The age of patients ranged from 41 to 80 years with the mean value of 61.7 years and standard deviation of 8.7 years. CT scanning was performed on a multi-slice Volume Zoom Siemens scanner with the standard clinical kV and mA settings during the one-breath hold. The voxel size of 9 tomograms was in the range of 0.65-0.74 mm in the axial image plane with the slice thickness equal to the inter-slice distance of 1.5 mm. The voxel size of 31 remaining tomograms was 0.68 mm in the axial image plane with the slice thickness equal to the inter-slice distance of 5.0 mm. No intravenous contrast agent was administered before the collection of scan data what is a significant detail of present study.

Quantitative assessment of the utility of generalized gradient maps in highlighting lung tumor borders was performed separately for the first subgroup of 31 native CT images with the slice thickness of 5.0 mm and remaining 9 images of the second subgroup with the slice thickness of about 1.5 mm. Typical examples of original CT image ROIs and corresponding gradient map regions are presented in Fig.5.

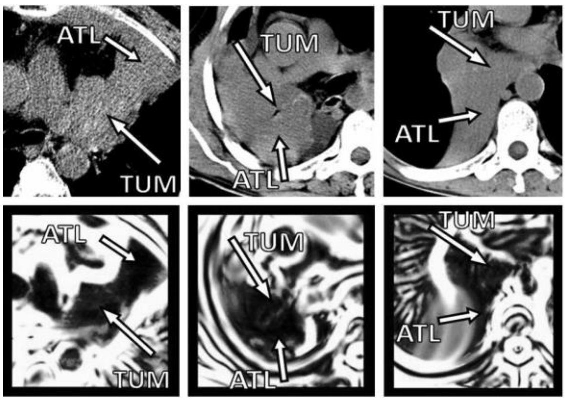

Fig. 5. Example ROIs of the original CT images of lungs (left column) and corresponding generalized gradient maps (right column). The first row represent case where the gradient map is definitely useful for detecting tumor border whereas the second and the third rows illustrate cases where the utility of maps is unclear and useless respectively.

As a result of the experiment, on the first subgroup of patients it was revealed that the generalized gradient maps were definitely useful for detecting tumor border in 17 patients (54.8%) whereas in 9 other cases (29.0%) they did not provide any help for solving the problem of separation the malignant tumor from adjacent atelectasis. The efficacy of maps in the rest 5 cases (16.1%) was found to be unclear. The results of the similar examination of CT scans with reasonably thin slices of about 1.5 mm suggest that it appears to be unlikely the slice thickness is an important parameter for the method. In particular, the distribution of cases between the “yes”, “no”, and “unclear” categories was 5 (55.6%), 3 (33.3%), and 1 (11.1%) respectively. This is well comparable with corresponding results obtained for the first subgroup.

4. CONCLUSIONS

In this paper, we have introduced the basic concept of so-called generalized gradient and demonstrated its abilities and key details on synthetic images, 3D CT images of physical phantom as well as CT scans of lung of 40 patients with clinically confirmed diagnosis of lung cancer.

5. REFERENCES

[1] M. Petrou, V. Kovalev, J. Reichenbach. Three-dimensional nonlinear invisible boundary detection, *IEEE Transactions on Image Processing* 15(10) (2006) p. 3020-3032

[2] V. Kovalev, M. Petrou. The classification gradient. *Proceedings of 18th International Conference on Pattern Recognition (ICPR-2006),* 3, Hong Kong, 20-24 August 2006, pp. 830-833

[3] M. Petrou, V. Kovalev, J. Reichenbach. High order statistics for tissue segmentation. *Handbook of Medical Image Processing and Analysis, 2nd edn.* Academic Press. San Diego, 2009. pp. 245-257

[4] M. Wedding, B. Gylys. *Medical Terminology Systems: A Body Systems Approach. 5th edn.* FA Davis Company. Philadelphia, 2004. p. 234.

[5] J. Mira, G. Fullerton, J. Ezekiel, J. Potter. Evaluation of computed tomography numbers for treatment planning of lung cancer. *International Journal of Radiation Oncology Biology Physics* 8(9) (1982) p. 1625-1628

[6] R. Wehrens, H. Putter, L. Buydens. The bootstrap: a tutorial. *Chemometrics and Intelligent Laboratory Systems* 54 (2000) p. 35-52